CHEMPHYSCHEM

ChemPubSoc Europe

DOI: 10.1002/cphc.201200201

Three Types of Induced Tryptophan Optical Activity Compared in Model Dipeptides: Theory and Experiment

Jana Hudecová,*[a, b] Jan Horníček,[a] Miloš Buděšínský,[a] Jaroslav Šebestík,[a] Martin Šafařík,[a] Ge Zhang,[c] Timothy A. Keiderling,[c] and Petr Bouř*[a]

The tryptophan (Trp) aromatic residue in chiral matrices often exhibits a large optical activity and thus provides valuable structural information. However, it can also obscure spectral contributions from other peptide parts. To better understand the induced chirality, electronic circular dichroism (ECD), vibrational circular dichroism (VCD), and Raman optical activity (ROA) spectra of Trp-containing cyclic dipeptides c-(Trp-X) (where X = Gly, Ala, Trp, Leu, nLeu, and Pro) are analyzed on the basis of experimental spectra and density functional theory (DFT) computations. The results provide valuable insight into the molecular conformational and spectroscopic behavior of Trp. Whereas the ECD is dominated by Trp π–π^* transitions, VCD is dominated by the amide modes, well separated from minor Trp contributions. The ROA signal is the most complex. However, an ROA marker band at 1554 cm^{-1} indicates the local χ_2 angle value in this residue, in accordance with previous theoretical predictions. The spectra and computations also indicate that the peptide ring is nonplanar, with a shallow potential so that the nonplanarity is primarily induced by the side chains. Dispersion-corrected DFT calculations provide better results than plain DFT, but comparison with experiment suggests that they overestimate the stability of the folded conformers. Molecular dynamics simulations and NMR results also confirm a limited accuracy of the dispersion-DFT model in nonaqueous solvents. Combination of chiral spectroscopies with theoretical analysis thus significantly enhances the information that can be obtained from the induced chirality of the Trp aromatic residue.

1. Introduction

The tryptophan (Trp) residue plays an important role in peptide conformational studies, especially those using chiral and fluorescence spectroscopic techniques.[1–6] The aromatic chromophore has an easily detectable spectral response. This is both convenient and a problem, as electronic circular dichroism (ECD) arising from Trp can interfere with that due to the peptide backbone and bias secondary structure analyses, while its fluorescence overlaps that of other aromatics. Coupling between Trp and other aromatic residues leads to a particularly large ECD that can be used for tertiary structure analyses.[7–11]

Trp also has distinctive vibrational spectral properties.[12,13] Its bands can be selectively enhanced in Raman spectra[2] and used for surface-enhanced studies.[14] Although the aromatic side chain in Trp is planar, strong Raman optical activity (ROA) features have been identified in some peptides and confirmed theoretically as being due to the chiral orientation of the adjacent covalent link.[15]

The Trp residue has many biological functions, including participation in ion transfer[16] and providing a signal or anchor for pores formed from transmembrane helices, which often terminate in Trp. Quinacrine drugs were suggested to interact with tryptophans.[17] Often, short secondary structures containing these residues are stabilized by a hydrophobic collapse.[18]

In this work, a series of small Trp-containing cyclic dipeptides was synthesized and subjected to spectroscopic and computational studies, in order to understand the side-chain role in the ECD, vibrational circular dichroism (VCD), and ROA spectra, and to monitor the Trp conformational properties in solution. The cyclic dipeptides (sometimes called 2,5-diketopiperazines, DKPs, after the central six-membered ring) are favored for model studies[19–21] as they are more rigid than linear peptides and are reasonably small, thereby facilitating the use of more accurate computations.

In particular, we were interested in the interaction of the Trp residue with the backbone and other side-chain parts of peptides, as such effects are crucial for developing ROA and ECD spectroscopic responses. As shown below, they provide complementary, but not identical, information about the structure to that obtained with NMR spectroscopy, which can be often reconciled only with complex theoretical modeling of molecu-

[a] J. Hudecová, J. Horníček, Dr. M. Buděšínský, Dr. J. Šebestík, M. Šafařík, Dr. P. Bouř
Institute of Organic Chemistry and Biochemistry
Academy of Sciences
Flemingovo náměstí 2, 16610 Prague 6 (Czech Republic)
Fax: (+420) 220183123
E-mail: hudecova@uochb.cas.cz
bour@uochb.cas.cz

[b] J. Hudecová
Institute of Physics, Faculty of Mathematics and Physics
Charles University
Ke Karlovu 5, 12116 Prague 2 (Czech Republic)

[c] G. Zhang, Dr. T. A. Keiderling
Department of Chemistry
University of Illinois at Chicago
845 W. Taylor St., Chicago, IL 60607-7061 (USA)

Supporting information for this article is available on the WWW under http://dx.doi.org/10.1002/cphc.201200201.

lar behavior. For symmetric molecules, such as the cyclic dipeptide c-(L-Trp-L-Trp), NMR spectroscopy cannot discriminate among the conformational variants of individual side chains, thus making the optical techniques, in particular ROA, in principle more suitable in this case.

However, the ROA spectral features are not necessarily local, and the side-chain contributions are mostly overlapped with the backbone signal.[22,23] Only some ROA bands can be associated with local molecular parts. Fortunately, for Trp, such a band exists at 1554 cm^{-1}, and its conformational dependence on the χ_2 side-chain dihedral angle can be reliably interpreted with computations.[15] For ECD, the Trp–Trp exciton coupling is generally believed to indicate a fixed and close mutual position. This was only partially confirmed by our modeling, as a large signal was observed in mono-Trp peptides (e.g. c-(Trp-Ala)) as well.

Peptide structural studies through chiral spectroscopies profit from the improved reliability and performance of the computational tools. The ECD spectra, for example, can be nowadays routinely simulated using time-dependent density functional theory (TDDFT)[24–26] for fairly large molecules, including the aromatic residues in peptides.[10,11]

Also, information about local molecular structure in the vibrational optical activity spectra can be fully grasped only when supported by the simulations.[27,28] For VCD theory, the most important milestones were perhaps the development of the magnetic field perturbation theory of Stephens,[29,30] and its implementation within the gauge-independent atomic orbitals (GIAOs)[31] and the DFT methodology.[32]

Similarly to VCD, the GIAOs should be used for ROA.[33] Although implemented within DFT,[34] ROA calculations have for a long time been hampered by the necessity to compute derivatives of some tensors numerically. This obstacle was lifted only recently by implementation of fully analytical schemes in publicly available programs.[35–40]

Our study also confirms the advantage of analysis of data from a combination of several spectroscopic techniques to characterize molecular behavior.[41,42] Especially, the vibrational methods provide new insight into details of peptide secondary structure.[43–48] However, the spectral interpretations and computations are still challenging, in particular for the proper representation of solvent involvement, conformational averaging, and balance of dispersion force.[49–51]

As indicated in previous studies the dispersion should be added to most DFT biomolecular studies.[52–56] This is true also for the Trp-containing dipeptides, although the benefit of the correction within a simplified solvent model may be limited.

Experimental Section

Synthesis: The synthesis started from N-protected (benzyloxycarbonyl, Z, and fluorenylmethoxycarbonyl, Fmoc) and C-protected (hydrochlorides of corresponding methyl esters) amino acids obtained from Merck, Czech Republic. Linear dipeptide precursors were prepared from Z-L-Trp-OH or Fmoc-D-Trp-OH and HCl·H-X-OMe peptides (X = Gly, Ala, Trp, Leu, nLeu, and Pro) using standard BOP activation[57] with 3 equiv diisopropylethylamine. Cyclic dipeptides c-(L-Trp-L-X) were obtained from Z-L-Trp-X-OMe, whereas c-(D-Trp-D-X) compounds were prepared from Fmoc-D-Trp-D-X-OMe, since different blocking groups were available for L- and D-Trp. The peptides were purified by column chromatography (Merck silica gel 60, $CHCl_3$/MeOH 25:1 or 10:1). Cyclization of the L series was achieved by 5 h of hydrogenolysis[58] on Pd sponge in MeOH with continual heating to 50 °C for 15–40 h. The Pd sponge was removed by filtration and washed with MeOH, acetonitrile (AcCN) or DMSO depending on the product solubility. The solvent was evaporated, and the product was crystallized several times from MeOH.

The cyclic D series peptides were obtained in two steps. First, the Fmoc group was removed using 1,8-diazabicyclo[5.4.0]undec-7-ene (DBU)/EtSH/AcCN (2:20:78) mixture[59] for 1 h, which was followed by extraction of the amine form between 1% HCl and diethyl ether. The aqueous solutions were adjusted to pH 8 with saturated $NaHCO_3$. Free amine was taken to EtOAc. After drying with Na_2SO_4 and evaporation of the solvent, the residue was heated in MeOH for 24–72 h. The precipitated cyclic form was filtered off and recrystallized from MeOH. In cases of low conversion, the remaining amino component was removed with Dowex-50 in MeOH.

Because of limited solubilities of the various cyclic dipeptides, a relatively wide range of solvents had to be used for the experimental NMR spectroscopy, ECD, VCD, and ROA, as summarized in Table 1.

Table 1. Overview of solvents used for the experimental spectra.

Compound	NMR	ECD	IR/VCD	Raman/ ROA
c-(L-Trp-Gly)	[D_6]DMSO, CD_3OD, $CDCl_3$	–	DMSO	DMSO
c-(D-Trp-Gly)	–	–	DMSO	DMSO
c-(L-Trp-L-Ala)	–	TFE, AcCN	–	–
c-(L-Trp-L-Trp)	[D_6]DMSO, CD_3OD	AcCN	DMSO, AcCN	DMSO, CH_3OH
c-(D-Trp-D-Trp)	–	AcCN	DMSO, AcCN	DMSO
c-(L-Trp-L-Leu)	[D_6]DMSO, CD_3OD	–	–	CH_3OH
c-(L-Trp-L-nLeu)	–	TFE, AcCN	–	–
c-(L-Trp-L-Pro)	[D_6]DMSO, CD_3OD	AcCN	DMSO, AcCN	–
c-(D-Trp-D-Pro)	–	AcCN	DMSO, AcCN	DMSO

NMR Spectroscopy: ^1H and ^{13}C NMR spectra of c-(L-Trp-Gly), c-(L-Trp-L-Trp), c-(L-Trp-L-Leu), and c-(L-Trp-L-Pro) were measured on a Bruker Avance II NMR spectrometer (^1H at 600.13 and ^{13}C at 150.9 MHz) equipped with a 5 mm cryo-probe. The spectra of all cyclic dipeptides were measured at 300 K in DMSO, CD_3OD, and $CDCl_3$. For structural assignment of proton and carbon signals (using natural ^{13}C occurrence), a combination of homo- and heteronuclear 2D NMR spectra (H,H-COSY, H,C-HSQC and H,C-HMBC) was used. The NOE contacts were determined from 2D H,H-ROESY spectra (mixing time 300 ms).

ECD Spectra: Electronic CD spectra for c-(L-Trp-L-Ala), c-(L-Trp-L-Trp), c-(D-Trp-D-Trp), c-(L-Trp-L-nLeu), c-(L-Trp-L-Pro), and c-(D-Trp-D-Pro) samples were measured using a Jasco J-810 spectropolarimeter. Samples were studied in 0.1 cm path length quartz cells,

using concentrations of about 0.2 mg mL^{-1} in AcCN or 2,2,2-trifluoroethanol (TFE). c-(Trp-Gly) was not sufficiently soluble under these conditions. Each spectrum was obtained as an average of six scans taken with a band pass of 1 nm and scanning speed of 50 nm min^{-1}. The experimental spectra are expressed in $\Delta\varepsilon$ (L mol^{-1} cm^{-1}); for this purpose the concentration was determined by the Trp UV absorption.

VCD Spectra: VCD spectra of the D and L forms of c-(Trp-Gly), c-(Trp-Trp), and c-(Trp-Pro) were measured using a homemade dispersive instrument separately described in detail.[60] The corresponding IR spectra were recorded on the same samples using a Vertex 80 FTIR (Bruker) spectrometer.

Samples were prepared by dissolving the peptides in DMSO or AcCN (not shown), to a concentration of about 10 mg mL^{-1}, and placing the solutions in a sealed cell composed of two CaF_2 windows separated by a 100 μm spacer. Spectra were obtained as the average of six scans and were corrected by subtraction of an identically obtained spectrum of the solvent. Most VCD signals were in general quite weak and comparable in intensity to the instrumental artifact signals developed with this high-refractive-index solvent. The VCD spectra are therefore presented as the difference of enantiomers, or (L−D)/2. Similarly, IR spectra are presented as their sum, or (L + D)/2.

ROA and Raman Spectra: All cyclic dipeptides were dissolved in DMSO or methanol to concentrations of 50–150 mg mL^{-1}, and the spectra were measured with a backscattering SCP BioTools μ-Chiral Raman-2X instrument equipped with an Opus diode-pumped solid-state laser operating at 532 nm.[61,62] The laser power was set to 50–100 mW, and power at the sample was 30–60 mW. Higher powers would cause a faster degradation of the samples. Residual fluorescence was quenched by leaving the sample in the laser beam for a few hours before measurement. The total acquisition time was about 20 h for each sample. For most samples, ROA spectra from two or three independent measurements were averaged. Solvent bands were subtracted from the Raman spectra, and minor baseline corrections were made. In the case of strong solvent scattering, affected wavenumber regions were deleted from the spectra. In this work we analyzed only the ROA of c-(Trp-Trp) and c-(Trp-Gly), where both enantiomers were available and measurable; the spectra are then presented as the difference (L−D)/2, as for VCD.

DFT Geometries: Lowest-energy conformations of selected dipeptides (Tables 2 and 3) were obtained by geometry optimization with the Gaussian program,[63] mostly using the B3LYP[64] functionals and 6-311 ++G** basis set. For some tests, the aug-cc-pVTZ standard basis sets, MP2,[65] MPW2PLYP,[54,66] B3PW91,[67] and BPW91[68] methods were used as specified below (Table S1, Supporting Information). The conductor-like polarizable continuum model (CPCM)[69] was used with AcCN (relative permittivity, $\varepsilon_r = 36$), $CHCl_3$ ($\varepsilon_r = 4.7$), TFE ($\varepsilon_r = 27$), CH_3OH ($\varepsilon_r = 33$), and DMSO ($\varepsilon_r = 47$) parameters for computations on the c-(L-Trp-L-Trp) molecule. The solvent variations, however, had only a minor effect on the resultant spectra and relative conformer energies, as documented in Figure S1 in the Supporting Information. For calculations of other molecules

Table 2. Selected geometry parameters,[a] relative energies,[b] and Boltzmann weights[c] of the most populated conformers,[d] calculated at the B3LYP/6-311 ++G**/CPCM(DMSO) level.

Conformation[e]		χ_1	χ_2	ϕ	ψ	ΔE	η
c-(Trp-Gly)							
A		−61	103	23	−16	0	35
A′		−60	106	−25	17	0.1	32
B		−59	−87	22	−16	0.7	11
D		62	−92	28	−19	0.7	11
C		63	89	25	−17	0.9	8
c-(Trp-Ala)							
A		−60	103	18	−12	0	39
A′		−60	106	−28	19	0.1	32
B		−59	−87	18	−13	0.7	11
B′		−57	−83	−25	15	1.1	6
D		63	−89	17	−12	1.1	6
C		63	90	14	−9	1.1	6
c-(Trp-Leu)							
A3	Trp	−61	103	15	−11	0	45
	Leu	−63	172	16	−11		
B3		−58	−88	18	−13	0.7	13
		−63	172	18	−14		
A8		−61	103	20	−15	0.9	9
		−167	64	27	−21		
D3		62	−89	16	−11	1.1	7
		−62	174	14	10		
C3		64	90	13	−9	1.2	6
		−63	173	16	−11		
c-(Trp-Trp)							
AA	Trp 1	−61	102	16	−10	0	25
	Trp 2	−61	102	16	−10		
A′A′		−59	105	−19	11	0.1	22
		−60	105	−19	12		
AB		−61	103	16	−11	0.7	15
		−58	−88	15	−10		
A′B′		−60	105	−12	6	1	10
		−58	−84	−10	5		
AD		−60	103	16	−10	0.9	11
		62	−90	17	−11		
c-(Trp-Pro)[f]	(P, Θ_m)						
A′ S	(302.4, 38.2)	−60	108	−37	31	0	64
B′ S	(302.7, 38.3)	−58	−82	−36	31	1	12
A′ N	(75.9, 36.1)	−59	108	−41	36	1.1	10
B′ S	(300.3, 38.1)	−63	−22	−39	33	1.5	5
C′ S	(303.9, 38.2)	54	80	−35	30	1.9	3

[a] Torsion angles χ_1, χ_2, ϕ, and ψ, in degrees, defined in Figure 1, for L,L enantiomers for DFT structures. [b] ΔE, in kcal mol^{-1}. [c] Including degeneracy; in %. [d] Conformers with relative energy $\Delta E < 2$ kcal mol^{-1} are specified. [e] Notation of peptide conformation is specified in Figure 2. [f] Type of proline puckering: S or N defined by phase P and amplitude Θ_m.

Table 3. Selected geometry parameters, relative energies, and Boltzmann weights of the most populated conformers, calculated at the B3LYP-D/6-311++G**/CPCM(DMSO) level.[a]

Conformation		χ_1	χ_2	ϕ	ψ	ΔE	η
c-(Trp-Gly)							
D		60	−90	37	−24	0	76
C		61	87	33	−23	0.7	23
c-(Trp-Ala)							
D		62	−90	24	−15	0	55
C		63	94	21	−11	0.1	43
c-(Trp-Leu)							
D3	Trp	64	−93	22	−18	0	64
	Leu	−50	−175	13	−9		
C3		65	91	18	−11	0.8	17
		−55	178	20	−13		
C8		61	98	20	−9	1.5	5
		−176	54	26	−15		
D2		64	−93	20	−15	1.6	4
		−74	64	20	−15		
c-(Trp-Trp)							
AD		−56	103	17	−8	0	66
		64	−89	22	−13		
BD		−64	−90	10	−1	0.8	19
		66	−81	23	−12		
BC		−59	−96	11	−7	1.7	4
		72	102	13	−4		
C′C′		67	92	−18	10	1.3	4
		64	83	−13	6		
D′D′		62	−83	−2	1	1.4	3
		56	−96	−16	12		
AC		−57	103	19	−10	1.8	3
		64	93	19	−10		
c-(Trp-Pro)	(P, Θ_m)						
D	(4.0, 39.7)	62	−91	26	−18	0	86
C	(326.8, 41.9)	65	88	21	−12	1.4	8

[a] Symbols same as in Table 2.

only the DMSO ε_r value (or $CHCl_3$ value for checking of conformer preference) was used with both the normal and dispersion-corrected (B3LYP-D)[54,66,70] B3LYP functional.

A two-dimensional scan was performed for c-(L-Ala-L-Ala) to investigate the inner ring potential energy surface (PES). Torsion angles ϕ and ψ (Figure 1, Table 4) were scanned in the range from −50° to +50° with a step of 5° at the B3LYP/CPCM(DMSO)/6-311++G** level. Because of the relatively simple single-valley PES that resulted from the 2D scan, for the other dipeptides we performed a relaxed 1D scan along the ϕ angle only.

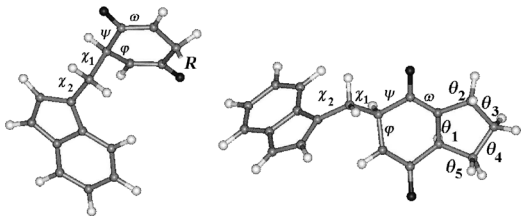

Figure 1. Characteristic coordinates of the c-(L-Trp-X), X = Gly, L-Ala, L-Leu, L-nLeu, L-Trp, and c-(L-Trp-L-Pro) cyclic dipeptides.

For c-(L-Trp-L-Trp) at the B3LYP/6-311G** level, the Trp side-chain conformation was investigated by a scan along torsion angles χ_1 and χ_2, from −180° to +165° with 15° increments; other coordinates were allowed to relax. This revealed four minima; the angle χ_1 favors values around −60° and 60°, and χ_2 prefers −90° and 90°.

Based on these scans, c-(L-Trp-Gly), c-(L-Trp-L-Ala), c-(L-Trp-L-Leu), c-(L-Trp-L-Trp), and c-(L-Trp-L-Pro) dipeptide geometries were generated with starting values χ_1 of about −60, 60, and 180°, $\chi_2 \approx -90$ and 90° (these conformations are depicted in Figure 2) together with two possible ring conformations, $\phi \approx -25°$ and 25°, and optimized by energy minimization (with B3LYP or B3LYP-D and CPCM-(DMSO)/6–311++G**). For c-(L-Trp-L-Trp), c-(L-Trp-L-Leu), and c-(L-Trp-L-Pro), the conformation of the second side chain was also investigated systematically; for Leu, the χ_1' and χ_2' torsion angles were set at −60°, 60° or 180° for beginning the optimization; similarly, we used the S and N conformations[71–74] of the proline five-membered ring.

Generation of the Spectra: Harmonic IR, VCD, Raman, and ROA intensities were computed with the Gaussian programs at the same level of theory as for optimized structures. The B3LYP functional with a medium-sized basis set has been found very convenient for analogous spectral simulations in many previous studies.[75–78] An excitation frequency of 532 nm was used for backscattered Raman and ROA dynamic (frequency-dependent) polarizabilities. Relative Raman and ROA spectral $S(\omega)$ shapes were obtained by convoluting the calculated intensities (I) with Lorentzian bands $\Delta = 8\ cm^{-1}$ wide, and multiplying by a temperature-correction factor for $T = 298$ K, so that the spectrum from each mode i can be represented as [Eq. (1)]:

$$S(\omega) = I\left[1 - \exp\left(-\frac{\omega_i}{kT}\right)\right]^{-1} \frac{1}{\omega_i}\left[4\left(\frac{\omega - \omega_i}{\Delta}\right)^2 + 1\right]^{-1} \quad (1)$$

Table 4. *R* on cyclic dipeptides.

R	peptide
−H	c-(L-Trp-Gly)
$-CH_3$	c-(L-Trp-L-Ala)
$-CH_2CH(CH_3)_2$	c-(L-Trp-L-Leu)
$-(CH_2)_3CH_3$	c-(L-Trp-L-nLeu)
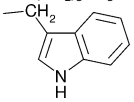	c-(L-Trp-L-Trp)

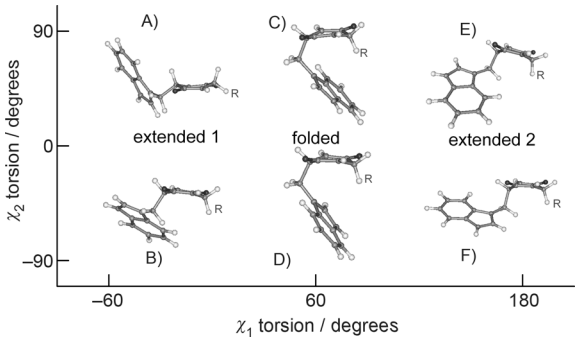

Figure 2. Conformational classes (A–F) of the Trp-containing dipeptides (see also Table 2 for conformer energies). The canonical angles (χ_1, χ_2, Figure 1) are A(−60, 90°), B(−60, −90°), C(60, 90°), D(60, −90°), E(180, 90°), and F(180, −90°).

where k is the Boltzmann constant and ω_i the vibrational frequency. Similarly, for VCD ($S(\omega)=\Delta\varepsilon$) and IR spectroscopy ($S(\omega)=\varepsilon$) [Eq. (2)]:

$$S(\omega) = cJ\frac{2\omega_i}{\Delta\pi}\left[4\left(\frac{\omega-\omega_i}{\Delta}\right)^2+1\right]^{-1} \quad (2)$$

where $S(\omega)$ is in units of $mol^{-1}L\,cm^{-1}$, J is the rotational/dipole strength in debyes^2, and $c=108$ for IR and 435 for VCD. Contributions of individual conformers were averaged using Boltzmann weights based on the sum of electronic and zero-point energies (ZPEs).

ECD spectra were generated from the dipole and rotational strengths calculated with Gaussian programs using the TDDFT method (B3LYP or B3LYP-D/CPCM(DMSO)/6-311++G**), and convoluted with Gaussian bands 15 nm wide. Surprisingly, the CAM-B3LYP[79] functional, sometimes claimed to be superior to B3LYP for ECD,[80] performed much worse for our system, and was thus not used.

Molecular Dynamics: An alternate solvent model was explored for c-(L-Trp-L-Trp) and c-(L-Trp-L-Pro), by running molecular dynamics (MD) simulations with the Amber10 program package[81] and using the Amber99 force field. Missing force-field parameters in the cyclic dipeptide ring were derived from a Hartree–Fock (HF)/6-31G* calculation with Gaussian, using the "POP=MK" keyword. DMSO and chloroform force fields were obtained from the extended Amber database (http://www.pharmacy.manchester.ac.uk/bryce/amber). The solute molecule was surrounded by solvent molecules (DMSO, methanol, chloroform, or water) up to a distance of 8–14 Å. A four-step equilibration[82] was carried out, followed by a 50 ns (100 ns for c-(L-Trp-L-Trp) in water) production run, using *NpT* ensembles and 1 fs integration time. Snapshots were taken each 5 ps and divided into three groups for c-(L-Trp-L-Trp) (folded: CC, CD, and DD; partially folded: AC, AD, BC, BD, CE, CF, DE, and DF; and extended: AA, AB, AE, AF, BB, BE, BF, EE, EF, and FF), and into two groups for c-(L-Trp-L-Pro) (folded: C, D; and extended: A, B, E, F; see Figure 2), according to the values of the χ_1 and χ_2 Trp angles. The relative conformer populations were normalized to 100%. From three independent MD runs for c-(L-Trp-L-Trp) the population error thus obtained was estimated as 20%.

2. Results and Discussion

Dipeptide Ring Geometry

It is known that the cyclic dipeptidic unit is normally quite flexible, and its conformation is very dependent on the amino acid side-chain type and interactions.[83] For example, c-(L-Ala-L-Ala) in a crystal is puckered, whereas c-(L-Ala-D-Ala) is nearly flat.[84] The peptide ring in the c-(L-Trp-L-Trp) crystal structure is also flat.[85] This is in agreement with the computed one- and two-dimensional PESs for c-(L-Ala-L-Ala), displayed in Figure 3.

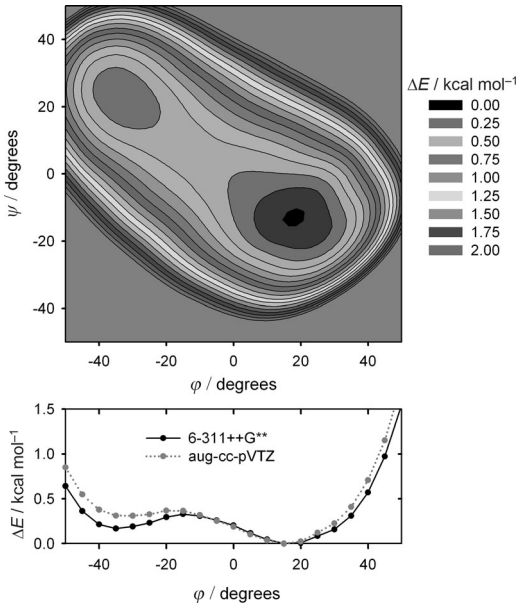

Figure 3. Top: calculated 2D (ϕ, ψ, B3LYP/CPCM(DMSO)/6-311++G**) PES for the inner ring in c-(L-Ala-L-Ala). Bottom: the corresponding 1D energy scan along the torsion angle ϕ [B3LYP/CPCM(DMSO)].

Clearly, the potential is shallow, and at 300 K ($kT\approx0.6$ kcal mol^{-1}) the ring is quite flexible, thus allowing for large deviations of the ψ and ϕ angles. The other principal angles in the dipeptide ring (ψ' and ϕ') adopt similar values to ψ and ϕ during the ring deformation. Minor variations were caused by the 6-311++G** and aug-cc-pVTZ basis set change (Figure 3, bottom). The flat ring-deformation potential is undoubtedly caused by a partial conjugation of the amide-bond π-electronic systems and strongly anharmonic out-of-plane amide deformation energy, as observed, for example, for the *N*-methylacetamide (NMA) molecule.[86]

Other peptides (c-(Gly-Gly), c-(L-Ala-L-Ala), c-(L-Ala-Gly), and c-(L-Leu-Gly)) showed a similar dependence (other 1D surfaces are shown in Figure S2, Supporting Information), although a closer look reveals finer differences between the dipeptides. Unlike c-(L-Ala-L-Ala), c-(Gly-Gly) exhibits two minima with the same energy, which reflects the symmetry of the molecule. The L-Leu enforces a stronger preference for the global minimum. The relative energies are notably changed by switching on the dispersion correction (bottom of Figure S2); if included, for ex-

ample, the difference in the two minima of c-(L-Ala-L-Ala) increases by ≈ 0.4 kcal mol^{-1} and the dipeptide ring becomes more twisted.

For c-(L-Trp-Gly), the relative energy differences between the two dipeptide ring conformers ($\phi \approx -40$ and 40°) also strongly depend on the conformation of the side chains, as documented in Figure S3 in the Supporting Information. For some conformers (C and D, Figure 2), the $\phi \approx -40^\circ$ minimum is missing; for A and B this minimum is very shallow.

Conformations of the Dipeptides

In Tables 2 and 3 we list the lowest-energy conformers ($\Delta E <$ 2 kcal mol^{-1}) for the c-(L-Trp-Gly), c-(L-Trp-L-Ala), c-(L-Trp-L-Leu), c-(L-Trp-L-Trp), and c-(L-Trp-L-Pro) dipeptides as obtained by a systematic conformer search. The B3LYP/CPCM(DMSO)/6-311++G** approximation level was used with (DFT-D) and without (DFT) correcting for the dispersion interactions.

The conformers can be approximately categorized according to the values of χ_1 and χ_2 as "extended" (marked as A, B, E, F), where the Trp indole side ring points out from the dipeptide ring, or "folded" (marked as C, D), where the Trp indole is above/below the ring, potentially stabilized by interaction with the other amino acid side chain (Figure 2).

Rather contradictory conformational analysis results are obtained with the DFT and DFT-D approaches (Tables 2 and 3), using the CPCM solvent model with DMSO parameters. When DMSO was replaced by chloroform in the model, only minor changes in conformer populations appeared (mostly less than ± 5%). Typically, the DFT method alone predicts that the extended conformers are most stable, with a minor but not negligible population (≈ 20%) of the folded ones. DFT-D almost exclusively favors the folded structures, separated from the extended ones by a wide energy margin. Interestingly, even the c-(L-Trp-Gly) is predicted to be entirely folded by DFT-D, although Gly does not possess any significant polarizable component beyond the DKP ring. The results are nevertheless consistent with previous studies, which clearly document the large effect of including the dispersion correction, and the significant energy changes computed with this force.[53,54,66,70,87]

For c-(L-Trp-Gly), Boltzmann populations obtained at other approximation levels (including B3LYP, BPW91, B3PW91, MP2, MPW2PLYP) are summarized in Table S1 in the Supporting Information. The uncorrected DFT results (B3LYP, BPW91, B3PW91) are very similar, and favor all the extended conformers A and A′. Likewise, the dispersion correction always switches the equilibrium to the folded structures C and D. The MP2 theory provides almost the same conformer distribution as the DFT-D methods. The MPW2PLYP results are also very similar to those from DFT-D; yet we see that some population of the A, A′, B, and B′ conformers (in total 20%) is allowed by the MPW2PLYP method, unlike for MP2 and DFT-D (< 1%). This reflects the well-known fact that the plain MP2 correction tends to overestimate the dispersion correction if compared to HF or older DFT formulations.[53,54,66]

NMR Results

NMR spectra allow for the use of more variable experimental conditions, in particular different kinds of solvents. In most cases NMR spectroscopy can monitor the conformation of a cyclic dipeptide, and verify theoretical structural predictions.[88,89] The analysis of the J(NH, $^\alpha$H) vicinal couplings and the resultant ϕ angles in [D_6]DMSO are summarized in Table 5.

Table 5. Experimental J(NH, $^\alpha$H) coupling constants [Hz] in DMSO, the inner-ring ϕ angle [°] in DMSO, MD-averaged ϕ values (for c-(L-Trp-L-Trp)) in DMSO, and Boltzmann-averaged ϕ values from DFT and DFT-D computations (B3LYP/CPCM(DMSO)/6-311++G**).

	c-(L-Trp-Gly)		c-(L-Trp-L-Leu)		c-(L-Trp-L-Pro)	c-(L-Trp-L-Trp)
	Trp	Gly	Trp	Leu	Trp	Trp
J	2.6	2.9; 0.9	2.6	2.9	≈ 0.8	2.9
ϕ_{exp}[a]	9	12	9	12	−37	12
ϕ_{MD}	–	–	–	–	−14	11
ϕ_{DFT}	7	5	16	18	−37	5
$\phi_{DFT\text{-}D}$	36	30	20	16	24	16

[a] Obtained from the coupling according to ref. [100], with coefficients $A = 7.0$, $B = -1.1$, $C = 0.55$.

Table 5 also includes averaged ϕ values from the MD run ϕ_{MD} (for c-(L-Trp-L-Trp) and c-(L-Trp-L-Pro)) and Boltzmann-weighted DFT and DFT-D (B3LYP/CPCM(DMSO)/6-311++G**) results. Except for c-(L-Trp-L-Pro), NMR data indicate a very flattened boat form of the dipeptide ring ($\phi = 9$–12°). This agrees better with the uncorrected DFT and MD values than with DFT-D, but for c-(L-Trp-L-Trp), the experimental values lie between the DFT and DFT-D results. For c-(L-Trp-L-Pro) an opposite pucker ($\phi = -37^\circ$) was determined by NMR spectroscopy than for the other dipeptides, in agreement with a previous observation for a similar c-(L-Phe-L-Pro) compound (-49°).[90] This value is also nicely reproduced by DFT ($\phi = -37^\circ$), but again not as well by DFT-D (Boltzmann average, $\phi = 24^\circ$).

The amino acid side-chain conformation can be deduced from the J($^\alpha$H, $^\beta$H) and NOE (NH, $^\beta$H) values. The coupling constants and resultant approximate populations of the χ_1 rotamers are listed in Table 6; the solvents included [D_6]DMSO, CD_3OD, and $CDCl_3$ (see also Table 1). Note that two β-protons (referred to as R and S) provide individual NMR signals. The NMR data thus indicate a significant preference for the folded rotamer (where $\phi \approx 60^\circ$) in c-(L-Trp-Gly) and c-(L-Trp-L-Leu). In the case of c-(L-Trp-L-Leu) this leads to strong shielding of the Leu $^\alpha$H (3.39 and 3.57 ppm) and $^\beta$H protons (0.62 and −0.05 ppm in DMSO, and 0.66 and −0.20 ppm in CD_3OD) due to a ring current effect of Trp. Folded conformers also prevail in c-(L-Trp-L-Pro), but only at about half the population, 46–52%; in $CDCl_3$ extended conformers are strongly preferred. These facts are somewhat inconsistent with the dipeptide ring analysis, in that they agree more with the DFT-D results than with DFT. Nevertheless, they can be explained by the overestimation of the effects of dispersion in the DFT-D method. In particular, the Trp residue is mostly folded, as predicted by DFT-D, but it does not deform the inner ring so much. This is

Table 6. Experimental $J(^{\alpha}H, ^{\beta}H)$ coupling constants [Hz] and χ_1-rotamer populations η [%].[a]

	c-(L-Trp-Gly) Trp			c-(L-Trp-L-Leu) Trp			Leu			c-(L-Trp-L-Pro) Trp			c-(L-Trp-L-Trp) Trp		
$^{\beta}H$	R		S	R		S	R		S	R		S	R		S
J, DMSO	4.7		4.6	4		4.8	9.4		4.7	4.7		5.8	4.3		6.6
J, CD_3OD	3.8		4.6	3.6		4.6	10		4.3	≈5		≈5	3.9		7.4
J, CD_3Cl_3	–		–	3.9		8	10.2		3.7	3.8		10.9	3.7		8
	AB	EF	CD	AB	EF	CD				AB	EF	CD	AB	EF	CD
χ_1 [°]	*−60*	*180*	*60*	*−60*	*180*	*60*	*−60*	*180*	*60*	*−60*	*180*	*60*	*−60*	*180*	*60*
η, DMSO [%]	21	17	62	10	23	67	75	17	8	20	34	46	15	43	42
η, CD_3OD [%]	11	16	73	5	21	74	83	12	5	23	25	52	11	53	36
η, $CDCl_3$ [%]	–	–	–	11	60	29	84	6	10	10	90	0	9	60	31

[a] According to ref. [101], $J(^{\alpha}H, ^{\beta}H) = 5.86 - 1.86\cos(\tau) + 3.81\cos(2\tau) + 0.37\sin(\tau)$, where $\tau = \measuredangle(^{\alpha}H, C, C, ^{\beta}H)$.

also consistent with the prevailing conformation in the c-(L-Trp-L-Trp) crystal, for example, where a T-shaped folded conformation was found (indicated as AD in Tables 2 and 3), but the inner ring is almost planar.[85] The NMR data for the Trp conformation in c-(L-Trp-L-Trp) are not usable for reliable prediction; because of the symmetry, the Trp residues are not resolved by NMR spectroscopy and are subject to fast conformer exchange.

The χ_2 Trp angle can in principle be derived from the observed NOE values. However, our measured data indicate strong NOE contacts of Trp R-$^{\beta}$H with both HN protons, thus implying a fast flipping around the $^{\beta}C-^{\gamma}C$ bond, which prevents a reliable prediction.

Molecular Dynamics

The MD simulations with explicit solvent provide an alternative to the DFT-D/CPCM model. In spite of the large error of the populations (≈20%, see the Experimental Section), the MD results (Table 7) clearly indicate a more complicated picture.

Table 7. Conformer populations [%] for c-(L-Trp-L-Trp) and c-(L-Trp-L-Pro) obtained by MD/Amber10 simulations in different solvents.

c-(L-Trp-L-Trp)	Population[a]		
	extended	partially folded	folded
water	1	92	7
DMSO	45	55	0
CH_3OH	7	93	0
$CHCl_3$	90	10	0

c-(L-Trp-L-Pro)	Population					
	extended conformation				folded	
χ_1	−60°		180°		60°	
	A	B	E	F	C	D
water	14	21	4	2	30	28
DMSO	8	8	8	3	45	28
CH_3OH	26	15	1	1	23	34
$CHCl_3$	41	45	0	0	11	3

[a] Folded conformers: CC, CD, and DD; partially folded: AC, AD, BC, BD, CE, CF, DE, and DF; and extended conformers: AA, AB, AE, AF, BB, BE, BF, EE, EF, and FF (see Figure 2).

Unlike with DFT-D/CPCM (Table 3), for c-(L-Trp-L-Trp) the extended structures may be additionally present in MD. In the low-polarity $CHCl_3$ environment the extended forms prevail (90%). On the other hand, more polar solvents (DMSO, H_2O, MeOH) strongly favor more compact forms, in agreement with the hydrophobic collapse known for some Trp-containing peptides. In water (first line in Table 7) even the fully stacked parallel L-Trp-L-Trp folded conformers appear (7%), but the edge-on-face L-Trp-L-Trp interaction is still more probable (92%), as commonly found in the Trp-containing peptides and proteins.[18,91–94]

The MD-predicted preferences of the Trp side-chain position for c-(L-Trp-L-Pro) are in agreement with the NMR results (Table 6), also favoring extended conformers in $CHCl_3$. For c-(L-Trp-L-Trp) the results cannot be compared to NMR data because of molecular symmetry. The behavior in CH_3OH is very similar to that in water according to MD, that is, the ratio of extended and folded conformers is close to 50:50. In DMSO the folded conformers slightly prevail in MD (73:27); in NMR the ratio was 46:54. Thus, we see that the MD simulations reveal finer solvent effects than DFT-D/CPCM, which had almost the same conformer ratios for all solvents, although the MD results are limited by the force field inaccuracy.

ECD Spectra

The experimental spectra of c-(L-Trp-L-Ala), c-(L-Trp-L-Trp), c-(L-Trp-L-nLeu), and c-(L-Trp-L-Pro) in AcCN are plotted in Figure 4. Due to interfering absorbance of DMSO in the UV region, it was necessary to employ different solvents for ECD than for the vibrational spectra (VCD and ROA). The ECD spectra for these molecules have the unique characteristic that they are dominated almost completely by the Trp contributions, even for DKPs with only one Trp residue. The differences between the ECD in AcCN and TFE (mostly ≈5 nm shift, but preserving the general shape, Figure S4, Supporting Information) were relatively minor, and less than the differences between the various molecules. Such solvent effects would be difficult to model.[95]

The c-(L-Trp-L-Pro) is the outlier, which corresponds to a distortion of the peptide ring and consequently the interaction of

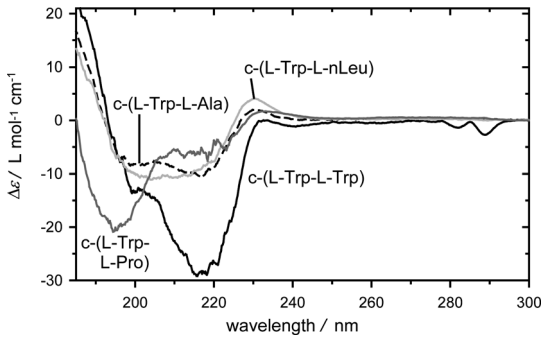

Figure 4. Experimental ECD spectra of c-(L-Trp-L-Ala), c-(L-Trp-L-Trp), c-(L-Trp-L-nLeu), and c-(L-Trp-L-Pro), all measured in AcCN. For analogous TFE results, see Figure S4 in the Supporting Information.

the Trp with the rest of the molecule caused by the constraints due to the Pro pyrrole ring. The near identical ECD for c(L-Trp-L-Ala) and c(L-Trp-L-Leu) suggests that the Trp is not interacting significantly with the aliphatic side chain, at least in these solvents. The much larger ECD seen for c-(L-Trp-L-Trp) in AcCN than for the other peptides (Figure 4) suggests a strong exciton coupling of the Trp residues,[11] and thus indicates a significant contribution from a stable interacting or folded conformation. This is further confirmed by the negative ECD at 290 nm, which is not seen for the other dipeptides.

The main features of the ECD spectra are reproduced for c-(L-Trp-L-Ala), c-(L-Trp-L-Trp), and c-(L-Trp-L-Pro) by the B3LYP/CPCM(DMSO)/6-311++G** computations (Figure 5). The averaging of contributions from thermally populated conformers had a minor influence on the total absorption, but had a major impact on the resultant averaged ECD, and consequently the DFT and DFT-D methods clearly provide very different ECD spectra (Figure 5). Individual conformer ECD (e.g. conformer C of c-(L-Trp-L-Ala) calculated with and without the dispersion, see Figure 5) are quite similar; thus, the resultant spectrum is mostly influenced by the weighting scheme dependent on the relative conformer energies (Tables 2 and 3).

For all molecules, it is clear that the conformer averaging is needed to obtain realistic spectral shapes and absolute intensities. It is also apparent that the balance of populated conformers changes the predicted ECD band shape by shifting the spectral band overlap, thus making the relative energetics more critical than the spectral prediction for each conformer.

IR and VCD Spectra

The experimental VCD and IR spectra of c-(L-Trp-Gly), c-(L-Trp-L-Trp), and c-(L-Trp-L-Pro) in DMSO are compared in Figure 6. We also measured spectra in other solvents, but in AcCN the c-(Trp-Trp) and c-(Trp-Pro) developed added bands which may be indicative of aggregation at IR concentrations. Such data are not presented. The amide I (C=O stretching, 1600–1700 cm^{-1}) IR spectrum has a relatively sharp band at 1670–80 cm^{-1} for c-(L-Trp-Gly) and c-(L-Trp-L-Trp), but the c-(L-Trp-L-Pro) exhibits a broadening due to the Trp–Pro link being a tertiary amide with a lower amide I frequency.[19,89] The main VCD signal is very weak and predominantly negative in the amide I region. It has some contributions from other underlying modes, which arise from the aromatic Trp side chain. The c-(L-Trp-L-Trp) molecule might have a positive couplet shape (+/−, from lower to higher frequency), but this is not clear in the experiment due to a baseline distortion.

The c-(L-Trp-L-Pro) VCD is surprisingly weak, considering the expected distortion of its peptide ring, with the amide I VCD being above but near to our measurement limits. (Most spec-

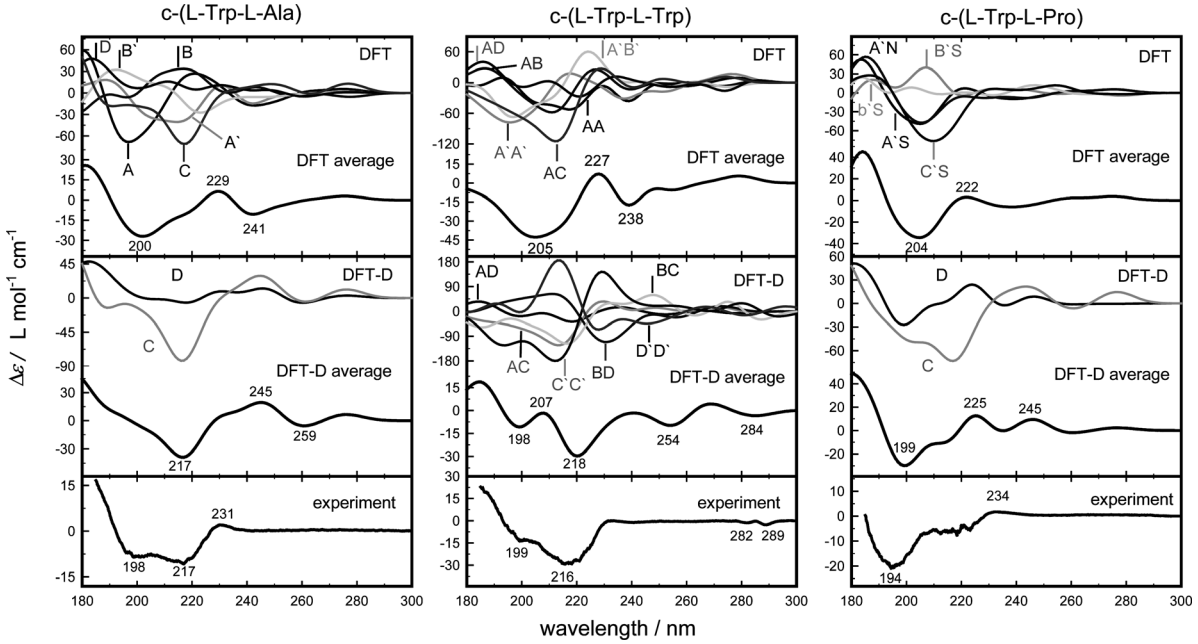

Figure 5. Calculated (B3LYP/CPCM(DMSO)/6-311++G**, DFT, and DFT-D geometries) and experimental ECD spectra of c-(L-Trp-L-Ala), c-(L-Trp-L-Trp), and c-(L-Trp-L-Pro). Relative abundances (Boltzmann weights) of different conformers are given in Tables 2 and 3.

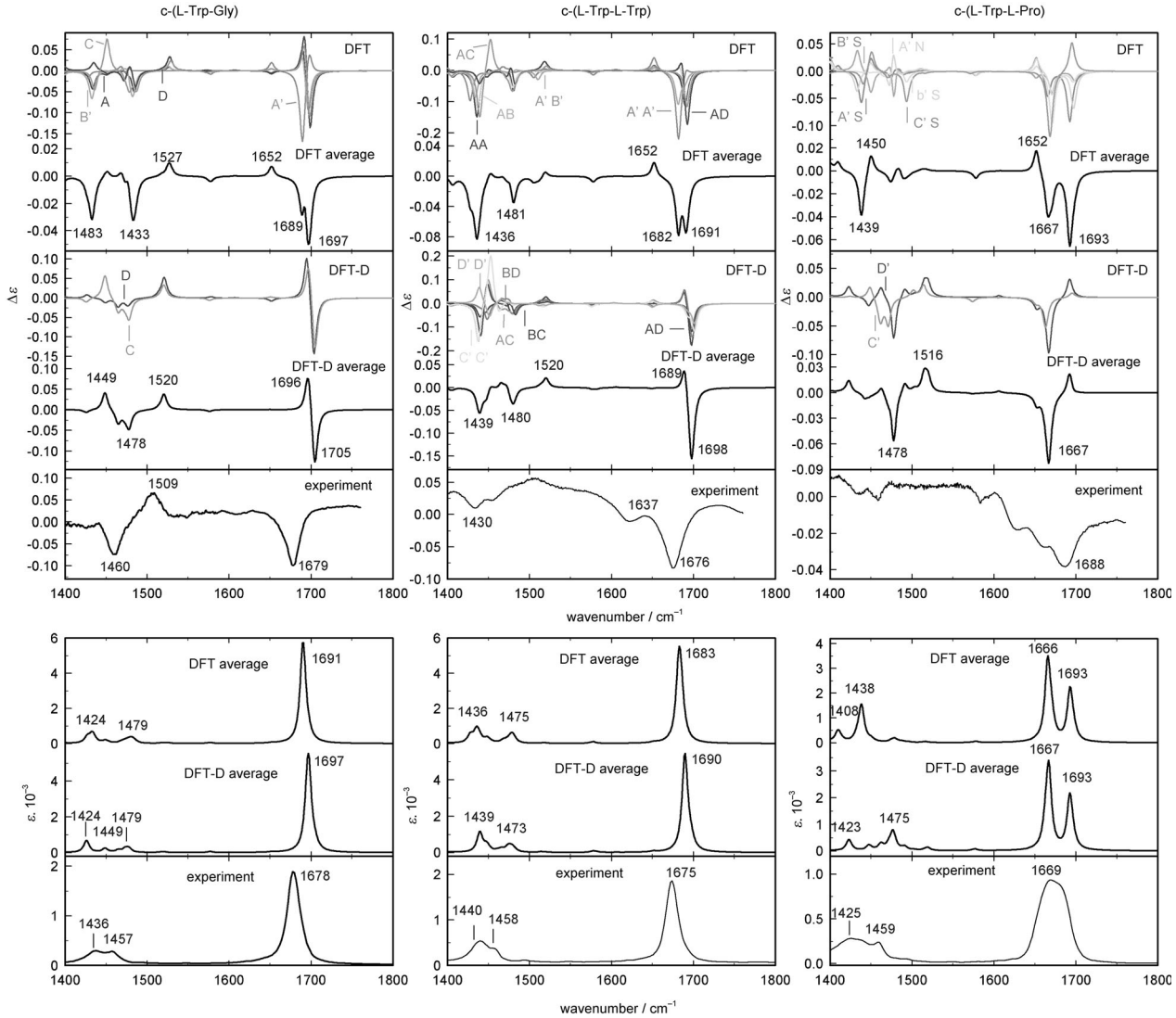

Figure 6. Calculated (B3LYP/CPCM(DMSO)/6-311++G**, DFT, and DFT-D) and experimental VCD and IR spectra of c-(L-Trp-Gly), c-(L-Trp-L-Trp), and c-(L-Trp-L-Pro) in DMSO. Experimental intensities are only approximate due to concentration error. Relative abundances (Boltzmann weights) of different conformers are given in Tables 2 and 3.

tra are measured with $A \approx 0.5$ for the amide I, so $\Delta\varepsilon/\varepsilon$ of 10^{-5} is above but close to our reliable measurement limit.) Such weak VCD spectra are subject to distortion through absorption artifacts, so that we limited our experimental VCD measurements to those samples for which we have both D,D and L,L isomers. In addition to amide I, there is a significant VCD signal arising from CH_2 motions and amide II bands (1430–1530 cm^{-1}), although this region is broader and more complex resulting in the IR and VCD patterns being less characteristic and not easily separable into local modes.[96]

The spectral simulations (Figure 6) reproduce many of the observed dependencies, with the IR and VCD predictions being very good aside from small frequency shifts as are expected for DFT. For example, in c-(L-Trp-Gly) the amide I VCD computed with the DFT calculation is predominantly negative. While many of the individual conformers have couplet amide I shapes, the negative lobes tend to dominate and, when weighted by population, prove to be the larger contributions.

The positive signal at 1652 cm^{-1} predicted by DFT might correspond to the very weak experimental feature at 1630 cm^{-1}. DFT-D provides a conservative couplet for amide I, in both C and D conformers, which does not reflect experiment. For the region 1400–1550 cm^{-1} (combination of CH_2 and amide II modes), on the other hand, neither method is in good agreement, but several conformers give rise to a positive band higher in frequency than a negative band, which is seen experimentally. After averaging, the DFT-D VCD curve is perhaps in better agreement with the experimental amide II than the DFT. The overlap and mixing of amide II (C-N-H deformation) and CH_2 modes is difficult to reproduce correctly by computations, as we have also found in previous model calculations.[97]

For c-(L-Trp-L-Trp) both DFT and DFT-D approaches provide the basic VCD pattern correctly (mostly negative amide I and a negative amide II region), although the calculated dispersion of the negative intensities around 1439 cm^{-1} is too large. In c-(L-Trp-L-Pro) the amide I VCD is predominantly negative and

broader than in c-(L-Trp-Gly) and c-(L-Trp-L-Trp), which is reproduced by the DFT calculations but not by the DFT-D results.

ROA Spectra

The ROA measurements were often hampered by the sample fluorescence (Table 1) and known instability of the Trp compounds in the (green) laser light.[98] The best experimental Raman and ROA spectra were obtained for 150 mg mL^{-1} (c-(L-Trp-L-Trp) and c-(D-Trp-D-Trp)) and 50 mg mL^{-1} (c-(L-Trp-Gly) and c-(D-Trp-Gly)) solutions in DMSO.

In Figure 7 the ROA and Raman spectra are shown, together with the corresponding DFT and DFT-D computations. The computations reproduce the strongest features in the observed Raman spectrum well. Both compounds have very similar Raman intensity patterns, which are dominated by the Trp modes (see the assignment in Table 8). Similar domination of the spectra by aromatic residues was observed previously for a model peptide.[22] The ROA spectra are more complex, but many observed features can be explained by the calculation. For example, the C=C five-membered Trp ring stretching band (experimentally at $\approx$1554 cm^{-1}) exhibits a negative ROA signal. This is, however, provided only by the dispersion model. On the other hand, DFT-D overestimates the relative intensity.

As discussed before,[15] although coming from the nonchiral chromophore, the ROA for this vibration is extremely sensitive to the Trp side-chain conformation, that is, the χ_2 angle. In particular, a negative ROA band is associated with conformations

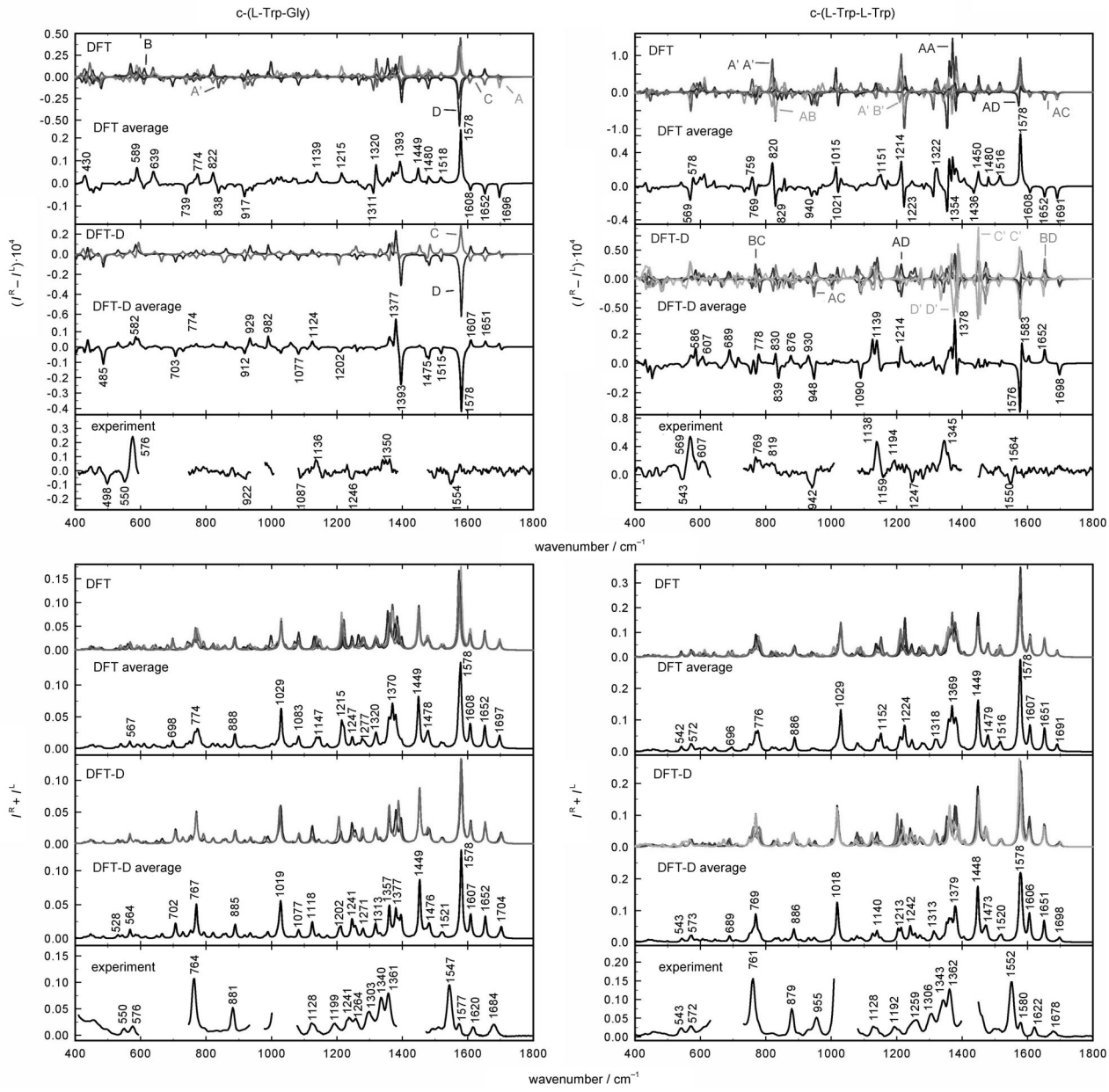

Figure 7. Calculated (B3LYP/CPCM(DMSO)/6-311++G**, DFT, and DFT-D geometries) and experimental ROA ($I_R - I_L$) and Raman ($I_R + I_L$) spectra of c-(L-Trp-Gly) and c-(L-Trp-L-Trp) in DMSO. The intensity of the experimental spectra is relative, only the ratio ROA/Raman is meaningful.

Table 8. Assignment of the most intense Raman bands.[a]

c-(Trp-Gly) DFT-D[b]	c-(Trp-Gly) Exp.	c-(Trp-Trp) Exp.	Vibrations
1704	1684	1678	A I, out of phase
1695	1684	1678	A I, in phase
1652	1620	1622	ν(C=C), ν(C=N) Trp
1607	1577	1580	ν(C=C), ν(C=N) Trp
1578	1547	1552	ν(C=C), Trp 5-membered ring
1449			amide II
1377	1361	1362	amide III
1357	1340	1343	ν(C=C), Trp
1312	1303	1306	Trp, 5-membered ring breathing
1271	1264	1259	ν(C=C), phenyl ring in Trp
1241	1241		ν(C=N) Trp, δ(CH)
1202	1199	1192	δ(CH), aliphatic
1118	1128	1128	ν(C–N) in amides
1019		$\approx$1020	ν(C=C), phenyl ring in Trp
982		955	ν(C–C) in amides, δ(CH)
885	881	879	ν(C=C), ν(C=N) Trp
767	764	761	ν(C=C), ν(C=N) Trp
564	576	572	ν(C=C), ν(C=N) Trp, out of plane amide NH
528	550	543	dipeptide ring deformation

[a] Frequencies in cm^{-1}. [b] B3LYP-D/CPCM(DMSO)/6-311++G** level.

with $\chi_2 \approx -90^\circ$, which is in agreement with the prevalent conformer population of this isomer predicted for c-(L-Trp-Gly) (Table 3). For c-(L-Trp-L-Trp) the prevalence of the T-shaped folded conformers with alternate ($+90^\circ$, -90°) χ_2 values causes partial cancelation and the resultant negative signal is smaller, which can be seen in both the theoretical and experimental ROA spectra.

Around 1350 cm^{-1} (CH bending, amide III) the predominantly positive experimental ROA signal is better reproduced by DFT-D for c-(L-Trp-L-Trp), but by DFT for c-(L-Trp-Gly). Within 1100–1250 cm^{-1} the experimental "$+-+-$" pattern seems to be better reproduced by DFT-D for both peptides. A negative ROA signal at 920–942 cm^{-1} is present in both experiments and all calculations. Below 900 cm^{-1}, the differences in the spectra provided by DFT and DFT-D are minor; nevertheless, both computations mostly reproduced the sign pattern observed experimentally. The large experimental positive ROA intensity at 576 and 569 cm^{-1} for c-(L-Trp-Gly) and c-(L-Trp-L-Trp), respectively, is not fully reproduced by the computation, which can be explained by an anharmonic character of the NH out-of-plane deformation.[99]

DFT versus DFT-D

To summarize the role of the dispersion at the spectral simulations, we can conclude that adding the physically correct van der Waals interaction significantly changes conformer equilibria. Most spectral features were improved when the dispersion was included, in line with similar investigations in the past.[52–56] However, there are also indications that only adding the correction to the dielectric solvent model may be an oversimplification. This is supported by the NMR data and the MD conformer ratios lying between DFT and DFT-D. Different spectral types (e.g. ECD, VCD, and ROA) also reacted differently in the dispersion correction; for VCD, for example, DFT-D provided bands that were too narrow due to the limited number of folded conformers. To better balance these complex dispersion, flexibility, and solvent effects remains a challenge for the future.

3. Conclusions

We have systematically compared the ECD, VCD, and ROA spectra of Trp-containing cyclic dipeptides. The results enable us to better understand the chiral spectral response of this residue in larger proteins and to characterize the link between the spectra and molecular structure. The Trp chromophore, although not intrinsically chiral if isolated from the backbone, dominated in the ECD and ROA dipeptide spectra. Especially surprising was the large Trp ECD signal of c-(L-Trp-L-Ala), as this molecule contains only one Trp residue without an exciton coupling between identical oscillators. Only for VCD can the interference between the side- and main-chain signals be avoided. However, the relative flatness of the ring makes the VCD weak and subject to artifacts.

The DFT computations provided a reliable basis for spectral interpretation. Dipeptide theoretical PESs, however, were strongly influenced by the presence or absence of the dispersion correction. Stable conformers yielded about the same spectra with DFT and DFT-D, but the dispersion energetically favored the compact folded forms. In general, the corrected computations also provided better spectra. Nevertheless, several indications appeared pointing to an overestimation of the dispersion effect within the CPCM solvent model. This was also confirmed by the NMR data and MD simulations, which revealed finer solvent effects, stemming from the solvent–solute dispersion and hydrogen bonding, that could be only partially included within DFT.

The chiral spectroscopies, at least in principle, eliminate the problems associated with measurements of symmetric molecules in solutions and unstable conformers by NMR spectroscopy. However, some experiments were hampered by limited solubility and instability of the dipeptides with Trp, and artifacts associated with the overlap with solvent vibrational bands. The ROA spectra appeared to be the most sensitive to the Trp side-chain conformation. Specific Trp marker bands could be found within the entire spectral region. In particular, the 1554 cm^{-1} ROA signal appeared useful as a unique local probe of the χ_2 angle, which is also otherwise difficult to monitor by other methods. Overall, we can conclude that the chiral spectroscopies provide very detailed information about the peptide structure, which must be, however, supported by theoretical modeling.

Acknowledgements

This study was performed with support from the Czech National Grant Agency (P208/11/0105), the Grant Agency of Charles Uni-

versity (126310), and the Ministry of Education (LH11033). The work at UIC was supported in part by a grant from the National Science Foundation (CHE 07 18543 to T.A.K.) and T.A.K. in part by a Research Award from the Alexander von Humboldt Stiftung.

Keywords: circular dichroism · conformation analysis · density functional calculations · peptides · Raman spectroscopy

[1] H. Edelhoch, *Biochemistry* **1967**, *6*, 1948 – 1954.
[2] R. P. Rava, T. G. Spiro, *J. Am. Chem. Soc.* **1984**, *106*, 4062 – 4064.
[3] L. S. Itzhaki, P. A. Evans, C. M. Dobson, S. E. Radford, *Biochemistry* **1994**, *33*, 5212 – 5220.
[4] S. M. O'Malley, M. J. McDonald, *J. Protein Chem.* **1994**, *13*, 561 – 567.
[5] E. Bismuto, I. Sirangelo, G. Irace, E. Gratton, *Biochemistry* **1996**, *35*, 1173 – 1178.
[6] C. P. Pan, M. D. Barkley, *Biophys. J.* **2004**, *86*, 3828 – 3835.
[7] R. W. Woody, *Eur. Biophys. J.* **1994**, *23*, 253 – 262.
[8] R. A. Sendak, D. M. Rothwarf, W. J. Wedemeyer, W. A. Houry, H. A. Scheraga, *Biochemistry* **1996**, *35*, 12978 – 12992.
[9] D. M. Rogers, D. M. Hirst, *Biochemistry* **2004**, *43*, 11092 – 11102.
[10] D. M. Rogers, N. A. Besley, P. O'Shea, J. D. Hirst, *J. Phys. Chem. B* **2005**, *109*, 23061 – 23069.
[11] A. Roy, P. Bouř, T. A. Keiderling, *Chirality* **2009**, *21*, E163 – E171.
[12] B. Hernández, F. Pfluger, A. Adenier, S. G. Kriglik, M. Ghomi, *J. Phys. Chem. B* **2010**, *114*, 15319 – 15330.
[13] S. D. Dieng, J. P. M. Schelvis, *J. Phys. Chem. A* **2010**, *114*, 10897 – 10905.
[14] A. E. Aliaga, I. Osorio-Roman, P. Leyton, C. Garrido, J. Carcamo, C. Caniulef, F. Celis, G. Diaz, E. Clavijo, J. S. Gomez-Jeria, M. M. Campos-Vallette, *J. Raman Spectrosc.* **2009**, *40*, 164 – 169.
[15] C. R. Jacob, S. Luber, M. Reiher, *ChemPhysChem* **2008**, *9*, 2177 – 2180.
[16] W. Hu, T. A. Cross, *Biochemistry* **1995**, *34*, 14147 – 14155.
[17] A. Saravanamuthu, T. J. Vickers, C. S. Bond, M. R. Peterson, W. N. Hunter, A. H. Fairlamb, *J. Biol. Chem.* **2004**, *279*, 29493 – 29500.
[18] A. G. Cochran, N. J. Skelton, M. A. Starovasnik, *Proc. Natl. Acad. Sci. USA* **2001**, *98*, 5578 – 5583.
[19] P. Bouř, V. Sychrovský, P. Maloň, J. Hanzlíková, V. Baumruk, J. Pospíšek, M. Buděšínský, *J. Phys. Chem. A* **2002**, *106*, 7321 – 7327.
[20] N. A. Besley, M. J. Brienne, J. D. Hirst, *J. Phys. Chem. B* **2000**, *104*, 12371 – 12377.
[21] J. Fleischhauer, J. Grötzinger, B. Kramer, P. Krüger, A. Wollmer, R. W. Woody, E. Zobel, *Biophys. Chem.* **1994**, *49*, 141 – 152.
[22] J. Hudecová, J. Kapitán, V. Baumruk, R. P. Hammer, T. A. Keiderling, P. Bouř, *J. Phys. Chem. A* **2010**, *114*, 7642 – 7651.
[23] S. Yamamoto, M. Straka, H. Watarai, P. Bouř, *Phys. Chem. Chem. Phys.* **2010**, *12*, 11021 – 11032.
[24] C. Jamorski, M. E. Casida, D. R. Salahub, *J. Chem. Phys.* **1996**, *104*, 5134 – 5147.
[25] F. Furche, R. Alhrichs, *J. Chem. Phys.* **2004**, *121*, 12772 – 12773.
[26] F. Furche, R. Ahlrichs, C. Wachsmann, E. Weber, A. Sobanski, F. Vögtle, S. Grimme, *J. Am. Chem. Soc.* **2000**, *122*, 1717 – 1724.
[27] L. A. Nafie, *Annu. Rev. Phys. Chem.* **1997**, *48*, 357 – 386.
[28] P. L. Polavarapu, *Chem. Rec.* **2007**, *7*, 125 – 126.
[29] P. J. Stephens, *J. Phys. Chem.* **1985**, *89*, 748 – 752.
[30] P. J. Stephens, *J. Phys. Chem.* **1987**, *91*, 1712 – 1715.
[31] K. L. Bak, F. J. Devlin, C. S. Ashvar, P. R. Taylor, M. J. Frisch, P. J. Stephens, *J. Phys. Chem.* **1995**, *99*, 14918 – 14922.
[32] J. R. Cheeseman, M. J. Frisch, F. J. Devlin, P. J. Stephens, *Chem. Phys. Lett.* **1996**, *252*, 211 – 220.
[33] T. Helgaker, K. Ruud, K. L. Bak, P. Joergensen, J. Olsen, *Faraday Discuss.* **1994**, *99*, 165 – 180.
[34] K. Ruud, T. Helgaker, P. Bouř, *J. Phys. Chem. A* **2002**, *106*, 7448 – 7455.
[35] V. Liégeois, K. Ruud, B. Champagne, *J. Chem. Phys.* **2007**, *127*, 204105.
[36] M. Pecul, K. Ruud, *Int. J. Quantum Chem.* **2005**, *104*, 816 – 829.
[37] K. Ruud, J. Thorvaldsen, *Chirality* **2009**, *21*, E54 – E67.
[38] J. R. Cheeseman, M. S. Shaik, P. L. A. Popelier, E. W. Blanch, *J. Am. Chem. Soc.* **2011**, *133*, 4991 – 4997.
[39] J. R. Cheeseman, M. J. Frisch, *J. Chem. Theory Comput.* **2011**, *7*, 3323 – 3334.
[40] J. R. Cheeseman in *Calculation of Molecular Chiroptical Properties Using Density Functional Theory*, University of Groningen, Groningen, **2007**, p. INV 3.
[41] P. L. Polavarapu, *Chirality* **2008**, *20*, 664 – 672.
[42] F. Wang, C. Zhao, P. L. Polavarapu, *Biopolymers* **2004**, *75*, 85 – 93.
[43] T. Weymuth, C. R. Jacob, M. Reiher, *ChemPhysChem* **2011**, *12*, 1165 – 1175.
[44] C. Herrmann, K. Ruud, M. Reiher, *ChemPhysChem* **2006**, *7*, 2189 – 2196.
[45] S. Yamamoto, J. Kaminský, P. Bouř, *Anal. Chem.* **2012**, *84*, 2440 – 2451.
[46] S. Luber, M. Reiher, *J. Phys. Chem. B* **2010**, *114*, 1057 – 1063.
[47] C. R. Jacob, S. Luber, M. Reiher, *J. Phys. Chem. B* **2009**, *113*, 6558 – 6573.
[48] C. Merten, L. D. Barron, L. Hecht, C. Johannessen, *Angew. Chem.* **2011**, *123*, 10149 – 10152; *Angew. Chem. Int. Ed.* **2011**, *50*, 9973 – 9976.
[49] M. Pecul, E. Lamparska, C. Capelli, L. Frediani, K. Ruud, *J. Phys. Chem. A* **2006**, *110*, 2807 – 2815.
[50] K. H. Hopmann, K. Ruud, M. Pecul, A. Kudelski, M. Dračínský, P. Bouř, *J. Phys. Chem. B* **2011**, *115*, 4128 – 4137.
[51] B. Mennucci, C. Cappelli, R. Cammi, J. Tomasi, *Chirality* **2011**, *23*, 717 – 729.
[52] I. Dabkowska, H. V. Gonzalez, P. Jurečka, P. Hobza, *J. Phys. Chem. A* **2005**, *109*, 1131 – 1136.
[53] S. Grimme, J. Antony, S. Ehrlich, H. Krieg, *J. Chem. Phys.* **2010**, *132*, 154104.
[54] S. Grimme, *J. Comput. Chem.* **2006**, *27*, 1787 – 1799.
[55] K. H. Hopmann, J. Šebestík, J. Novotná, W. Stensen, M. Urbanová, J. Svenson, J. S. Svendsen, P. Bouř, K. Ruud, *J. Org. Chem.* **2012**, *77*, 858 – 869.
[56] X. Li, K. H. Hopmann, J. Hudecová, W. Stensen, J. Novotná, M. Urbanová, J. S. Svendsen, P. Bouř, K. Ruud, *J. Phys. Chem. A* **2012**, *116*, 2554 – 2563.
[57] J. Ježek, R. Markošová, *Collect. Czech. Chem. Commun.* **1994**, *59*, 671 – 706.
[58] E. Wünsch, *Methoden der Organischen Chemie (Houben-Weyl)*, Thieme, Stuttgart, **1974**.
[59] J. E. Sheppeck, H. Kar, H. Hong, *Tetrahedron Lett.* **2000**, *41*, 5329 – 5333.
[60] A. Lakhani, A. Roy, M. De Poli, M. Nakaema, F. Formaggio, C. Toniolo, T. A. Keiderling, *J. Phys. Chem. B* **2011**, *115*, 6252 – 6264.
[61] W. Hug, G. Hangartner, *J. Raman Spectrosc.* **1999**, *30*, 841 – 852.
[62] W. Hug, *Appl. Spectrosc.* **2003**, *57*, 1 – 13.
[63] Gaussian 09 (Revision B01), M. J. Frisch, G. W. Trucks, H. B. Schlegel, G. E. Scuseria, M. A. Robb, J. R. Cheeseman, G. Scalmani, V. Barone, B. Mennucci, G. A. Petersson, H. Nakatsuji, M. Caricato, X. Li, H. P. Hratchian, A. F. Izmaylov, J. Bloino, G. Zheng, J. L. Sonnenberg, M. Hada, M. Ehara, K. Toyota, R. Fukuda, J. Hasegawa, M. Ishida, T. Nakajima, Y. Honda, O. Kitao, H. Nakai, T. Vreven, J. Montgomery, J. E. Peralta, F. Ogliaro, M. Bearpark, J. J. Heyd, E. Brothers, K. N. Kudin, V. N. Staroverov, R. Kobayashi, J. Normand, K. Raghavachari, A. Rendell, J. C. Burant, S. S. Iyengar, J. Tomasi, M. Cossi, N. Rega, J. M. Millam, M. Klene, J. E. Knox, J. B. Cross, V. Bakken, C. Adamo, J. Jaramillo, R. Gomperts, R. E. Stratmann, O. Yazyev, A. J. Austin, R. Cammi, C. Pomelli, J. W. Ochterski, R. L. Martin, K. Morokuma, V. G. Zakrzewski, G. A. Voth, P. Salvador, J. J. Dannenberg, S. Dapprich, A. D. Daniels, O. Farkas, J. B. Foresman, J. V. Ortiz, J. Cioslowski, D. J. Fox, Gaussian, Inc., Pittsburgh, PA, **2009**.
[64] A. D. Becke, *J. Chem. Phys.* **1993**, *98*, 5648 – 5652.
[65] C. Møller, M. S. Plesset, *Phys. Rev.* **1934**, *46*, 618 – 622.
[66] T. Schwabe, S. Grimme, *Phys. Chem. Chem. Phys.* **2007**, *9*, 3397 – 3406.
[67] J. P. Perdew, K. Burke, Y. Wang, *Phys. Rev. B* **1996**, *54*, 16533 – 16539.
[68] A. Becke, *Phys. Rev. A* **1988**, *38*, 3098 – 3100.
[69] J. Tomasi, B. Mennucci, R. Cammi, *Chem. Rev.* **2005**, *105*, 2999 – 3093.
[70] S. Grimme, *J. Comput. Chem.* **2004**, *25*, 1463 – 1473.
[71] J. Kapitán, V. Baumruk, V. Kopecký, Jr., P. Bouř, *J. Am. Chem. Soc.* **2006**, *128*, 2438 – 2443.
[72] J. Kapitán, V. Baumruk, V. Kopecký, Jr., R. Pohl, P. Bouř, *J. Am. Chem. Soc.* **2006**, *128*, 13451 – 13462.
[73] C. Altona, M. Sundaralingam, *J. Am. Chem. Soc.* **1972**, *94*, 8205 – 8212.
[74] S. J. Han, Y. K. Kang, *J. Mol. Struct.: THEOCHEM* **1996**, *369*, 157 – 165.
[75] E. E. Zvereva, A. R. Shagidullin, S. A. Katsyuba, *J. Phys. Chem. A* **2011**, *115*, 63 – 69.
[76] M. Reiher, V. Liegeois, K. Ruud, *J. Phys. Chem. A* **2005**, *109*, 7567 – 7574.
[77] J. Haesler, I. Schindelholz, E. Riguet, C. G. Bochet, W. Hug, *Nature* **2007**, *446*, 526 – 529.

[78] S. Yamamoto, H. Watarai, P. Bouř, *ChemPhysChem* **2011**, *12*, 1509 – 1518.
[79] T. Yanai, D. Tew, N. C. Handy, *Chem. Phys. Lett.* **2004**, *393*, 51 – 57.
[80] O. Julínek, M. Krupička, W. Lindner, M. Urbanová, *Phys. Chem. Chem. Phys.* **2010**, *12*, 11487 – 11497.
[81] D. A. Case, I. T. E. Cheatham, T. Darden, H. Gohlke, R. Luo, J. K. M. Merz, A. Onufriev, C. Simmerling, B. Wang, R. Woods, *J. Comput. Chem.* **2005**, *26*, 1668 – 1688.
[82] Z. Vokáčová, J. Šponer, J. E. Šponer, V. Sychrovský, *J. Phys. Chem. B* **2007**, *111*, 10813 – 10824.
[83] A. P. Mendham, T. J. Dines, M. J. Snowden, B. Z. Chowdhry, *J. Raman Spectrosc.* **2009**, *40*, 1478 – 1497.
[84] E. Sletten, *J. Am. Chem. Soc.* **1970**, *92*, 172 – 177.
[85] G. D. Grant, A. L. Hunt, P. J. Milne, H. M. Roos, J. A. Joubert, *J. Chem. Crystallogr.* **1999**, *29*, 435 – 447.
[86] V. Andrushchenko, P. Matějka, D. T. Anderson, J. Kaminský, J. Horníček, L. O. Paulson, P. Bouř, *J. Phys. Chem. A* **2009**, *113*, 9727 – 9736.
[87] V. Parchaňský, P. Matějka, B. Dolenský, M. Havlík, P. Bouř, *J. Mol. Struct.* **2009**, *934*, 117 – 122.
[88] M. J. O. Anteunis, *Bull. Soc. Chim. Belg.* **1978**, *87*, 627 – 650.
[89] M. Buděšínský, J. Symerský, J. Ječný, J. van Hecke, N. Hosten, M. J. O. Anteunis, F. Borremans, *Int. J. Pept. Protein Res.* **1992**, *39*, 123 – 130.
[90] M. Buděšínský, I. Císařová, J. Podlaha, F. Borremans, J. C. Martins, M. Waroquier, E. Pauwels, *Acta Crystallogr. Sect. B* **2010**, *66*, 662 – 677.
[91] R. Huang, L. Wu, D. McElheny, P. Bouř, A. Roy, T. A. Keiderling, *J. Phys. Chem. B* **2009**, *113*, 5661 – 5674.
[92] P. Bouř, T. A. Keiderling, *J. Phys. Chem. B* **2005**, *109*, 23687 – 23697.
[93] W. Y. Yang, J. W. Pitera, W. C. Swope, M. Gruebele, *J. Mol. Biol.* **2004**, *336*, 241 – 251.
[94] S. J. Russell, T. Blandl, N. J. Skelton, A. G. Cochran, *J. Am. Chem. Soc.* **2003**, *125*, 388 – 395.
[95] J. Šebek, Z. Kejík, P. Bouř, *J. Phys. Chem. A* **2006**, *110*, 4702 – 4711.
[96] T. A. Keiderling, J. Kubelka, J. Hilario in *Vibrational Circular Dichroism of Biopolymers: Summary of Methods and Applications* (Eds.: M. Braiman, V. Gregoriou), CRC, Boca Raton, **2006**, pp. 253 – 324.
[97] J. Kubelka, T. A. Keiderling, *J. Phys. Chem. A* **2001**, *105*, 10922 – 10928.
[98] K. Huvaere, L. H. Skibsted, *J. Am. Chem. Soc.* **2009**, *131*, 8049 – 8060.
[99] C. N. Tam, P. Bouř, J. Eckert, F. R. Trouw, *J. Phys. Chem. A* **1997**, *101*, 5877 – 5884.
[100] J. M. Schmidt, M. Blümel, F. Löhr, H. Rüterjans, *J. Biomol. NMR* **1999**, *14*, 1 – 12.
[101] J. M. Schmidt, *J. Biomol. NMR* **2007**, *37*, 287 – 301.

Received: March 8, 2012
Revised: April 27, 2012
Published online on June 15, 2012

